SAND2022-7242C

Multiple Inverter Microgrid Experimental Fault Testing

Nicholas S. Gurule, Javier Hernandez Alvidrez, Matthew J. Reno, and Jack Flicker
Sandia National Laboratories, Albuquerque, New Mexico, 87185, USA

***Abstract*—For the resiliency of both small and large distribution systems, the concept of microgrids is arising. The ability for sections of the distribution system to be "self-sufficient" and operate under their own energy generation is a desirable concept. This would allow for only small sections of the system to be without power after being affected by abnormal events such as a fault or a natural disaster, and allow for a greater number of consumers to go through their lives as normal. Research is needed to determine how different forms of generation will perform in a microgrid, as well as how to properly protect an islanded system. While synchronous generators are well understood and generally accepted amongst utility operators, inverter-based resources (IBRs) are less common. An IBR's fault characteristic varies between manufacturers and is heavily based on the internal control scheme. Additionally, with the internal protections of these devices to not damage the switching components, IBRs are usually limited to only 1.1-2.5p.u. of the rated current, depending on the technology. This results in traditional protection methods such as overcurrent devices being unable to "trip" in a microgrid with high IBR penetration. Moreover, grid-following inverters (commonly used for photovoltaic systems) require a voltage source to synchronize with before operating. Also, these inverters do not provide any inertia to a system. On the other hand, grid-forming inverters can operate as a primary voltage source, and provide an "emulated inertia" to the system. This study will look at a small islanded system with a grid-forming inverter, and a grid-following inverter subjected to a line-to-ground fault.**

Keywords— Microgrid, Inverter, Fault, Grid-Forming, Distributed Energy Resource, Volt-Var, Frequency-Watt

I. Introduction

It has been demonstrated that inverter-based resources (IBRs) are usually not capable of producing the necessary amounts of fault current, removing overcurrent protection as a viable option for heavily inverter-based microgrids. Other options such as negative-sequence current detection are becoming a more popular option as a protection scheme. However, dependent on the control scheme of an IBR, negative- or zero-sequence current may not be produced by a device during a fault. Specifically, it has been shown that a grid-following inverter (GFLI), commonly used for photovoltaic (PV) installations, that operates as a near-ideal, balanced current source, does not output a significant amount of negative- or zero-sequence current due to the controls. Grid-forming inverters (GFMIs) can be capable of outputting unbalanced currents depending on the control scheme, a needed feature if the intent for one of these devices is to operate as the primary source of a system.

While some work has been done to investigate the fault characteristics of a single device, or with multiple simulated/prototype devices [1]-[6], this study intends to look into the interaction of a commercially available GFMI and GFLI in a small islanded system after a single line to ground fault is applied to the system. While the GFMI will operate as the primary source and be set to operate with a droop characteristic (similar to that of a synchronous generator), the GFLI will be operating as an auxiliary source; either set to a fixed power or grid support functions (GSF) in the form of volt-var (VV) and frequency-watt (FW) control.

II. Background

GFMIs have been around for decades, originally being used for remote, standalone systems. However, these devices never gained popularity as they were too large for localized generation and could not operate with the grid, only working after the power went out. However, with an increase in electricity costs and tax incentives for the installation of PV, GFLIs have been placed throughout the distribution system. As the name implies, GFLIs follow the grid voltage, and therefore require a voltage and frequency reference to be present to operate. When the power goes out the inverter will not provide power to the system. Now with "modern" control schemes for GFMIs, grid synchronization is possible, and the device can act as either a grid support unit (providing real and reactive power when there is a deviation in the voltage and current) or operate as a primary source for a local system. Depending on the size of the GFMI, this system could be a single home, a neighborhood, or small town or city.

Both of these technologies have their own advantages and disadvantages. The growing penetration of PV inverters on the distribution system has resulted in the increased requirements for grid interconnection of GFLIs. This includes the addition of GSFs to the capability of the inverters (as well as voltage and frequency ride-through capability). GSFs help to maintain a stable grid under normal operating conditions, while event ride-through allows for GFLIs to continue operating (up to a certain point) during abnormal operating conditions (such as faults) to ensure that a potentially large amount of generation does not trip prematurely. GFMIs usually use some form of droop characteristic to maintain synchronization with the utility or other grid-forming devices [7],[8] and through this droop can also provide a form of grid support similar to that of the GFLIs. Both these systems are also capable of responding to events very quickly, much faster than traditional rotating generation. This quick response capability is very beneficial in a high inertia system, like the utility.

While the advantages of IBRs are attractive, there are a few shortcomings that should not be overlooked. First, GFLIs are commonly used with intermittent resources. Solar and wind resources are not always present, and thus are not a reliable form of generation. A GFMI is usually used for an energy storage system (ESS), and therefore as long as the ESS is charged (charged when excess generation is available and only

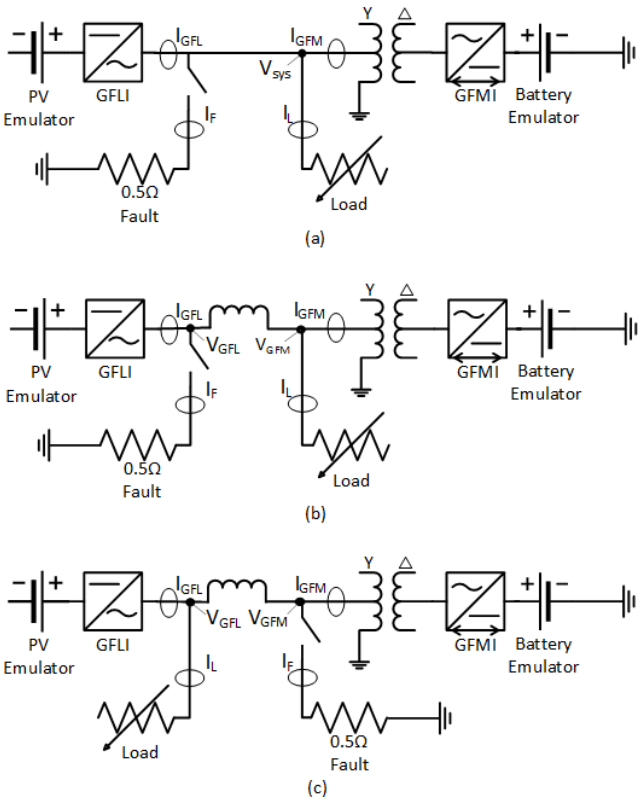

Fig. 1: Experimental Lab Test Configurations, Single Bus Fault (a), GFLI Side Fault (b), and GFMI Side Fault (c)

discharged when needed), the resource is reliable. Additionally, a disadvantage to an IBR is the sensitive components that they are comprised of. The circuitry of these devices has a maximum current limit, and thus has internal controls to protect these components. This results in devices that can only output slightly above rated current to usually no more than 3 p.u. during faults, and only if the headroom is available.

While the slow response of synchronous generators is not preferred, this response is well known and has been modeled and observed on both grid-tied and islanded systems. The effects of increased penetration of IBRs have been studied, as well as their effectiveness as a grid support device in both grid-tied [9] and microgrid applications. However, little work has been performed to determine how commercially available GFLIs and GFMIs interact in a high-IBR penetration islanded system (or in a fully IBR system).

III. Experimental Setup

For this study, a commercially available 24 kW GFLI and 100 kW GFMI were used as the IBRs. A 0-150 kW programmable resistive delta configured load was used as an aggregate load for the system. A 150 kW single-phase load was used as a fault (~0.5 ohms to ground).

Three test configurations were utilized for this study as shown in Fig. 1. The first was a single bus system, where all sources and loads were connected directly together, with no additional line impedance added to the system and all lines being less than 50 m. The other two configurations had a 1 mH inductance added to each of the three-phase lines between the two IBRs to emulate an extended line length, roughly 500 m of the largest conductor used in the system. For each of these configurations, the locations of the load and fault was reversed, i.e., the first configuration had the fault on the GFLI side with the load on the GFMI side, and the second the opposite.

For DC sources, the GFLI was connected to an Ametek TerraSAS 100 kW photovoltaic emulators, set to operate 1.25 p.u. of the rated power of the inverter. The GFMI was connected to an NH Research 9300 100 kW battery emulator as the DC source.

The GFMI requires an external delta/wye transformer for both isolation as well as achieving common system voltage. This IBR operated as the voltage source of the system was set to have a droop of 1% for both voltage and current, with a priority for real power output. No additional bias was set to the voltage and frequency, so at nominal system voltage (277/480 V) and frequency (60 Hz), the inverter should not output any power.

For each test configuration, the GFLI was first tested with all GSF off, followed by having both VV and FW functions enabled. The device is factory set to have reactive power priority, and can not be set for real power priority. With GSF enabled, the slopes were set to 1% with no deadband to match the characteristics of the GFMI. Additionally, the FW profile was evaluated at 0.5 p.u. and 1.0 p.u. initial output powers when operating at nominal frequency. These are seen in Fig. 2.

The load of the system was also varied for each test configuration. For each case, at least 24 kW of load was present on the system (to match the power rating of the GFLI). Further, tests were performed with an additional 25 kW load to the system to represent a quarter of the power rating of the GFMI rating. Additional load cases would have been evaluated,

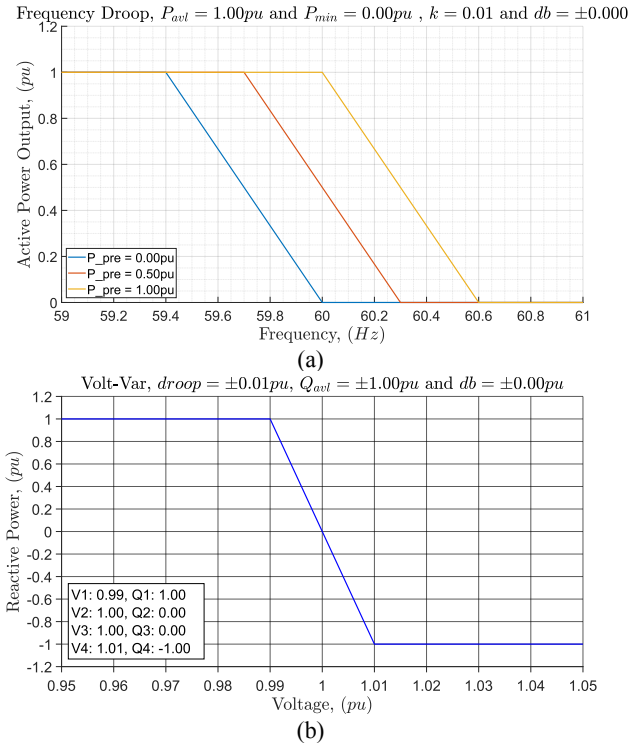

Fig. 2: GFLI Grid Support Function Profiles for a) frequency-watt, and b) volt-var

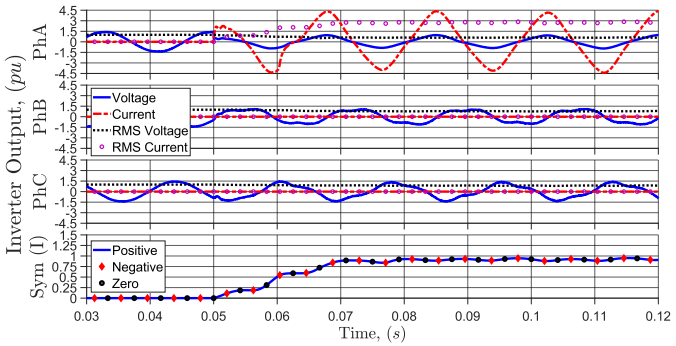

Fig. 3: GFMI Subjected to 150kW Single Line Fault

however the battery emulator tripped and stopped exporting power due to overloading during the fault event.

For each test case, a single-line-to-ground Phase A fault was applied to the system for at least 0.5s, but no longer than 2s. A single line-to-ground fault was chosen for this testing as it is the most prevalent fault to occur within any system. This was to ensure that the system could reach steady-state during the fault but not inadvertently trip the GFLI due to a low voltage or frequency event.

IV. Experimental Results

A. Configuration A

To first see if GFLIs can help an islanded system during a fault, the GFMI was first subjected to the fault without the GFLI present. For this initial test, no additional load was applied to the GFMI. Fig. 3 shows the response of the GFMI. An initial observation is that althrough the fault was only applied to phase A on the GFMI, all three phases were affected by the event. This is a trend seen throughout the tests to follow. Once the inverter response reached stability, the Phase A voltage of the GFMI was measured at an average of 0.536 p.u. with an average fault current contribution of 2.462 p.u. and a peak of 2.960 p.u. immediately after the onset of the fault. This is on par with what is known for the overload capability of GFMIs. Sensitive components internal to the IBR would need to be greatly oversized for higher levels of fault current to be achieved, so inverter controls are designed to protect the components by limiting the output current.

The GFLI was then added to the system, and a load of 24kW was initially placed onto the system to offset the power output of the GFLI. This allowed the GFMI to remain unloaded for a fair comparison to the previous test. For this first test with the GFLI, no GSFs were enabled. However, at the onset of the fault, the GFLI went into momentary cessation due to its low voltage ride-through settings. Because of this, the Phase A voltage drops to 0.511 p.u. and the GFMI must support both the load and fault, requiring a current output of 2.473 p.u. Following the removal of the fault, the inverter recovered to prefault conditions within 500ms. While this no longer posed as a good comparison with the previous test, it does show that knowing how an inverter responds to faults is crucial. For the tests to follow, the low voltage ride-through settings were adjusted to ensure that the GFLI would continue to operate during the fault.

With new settings, the test was rerun to get the desired comparison. Now that the GFLI does not go into momentary cessation, as seen in Fig. 4, an increase in system voltage, up to

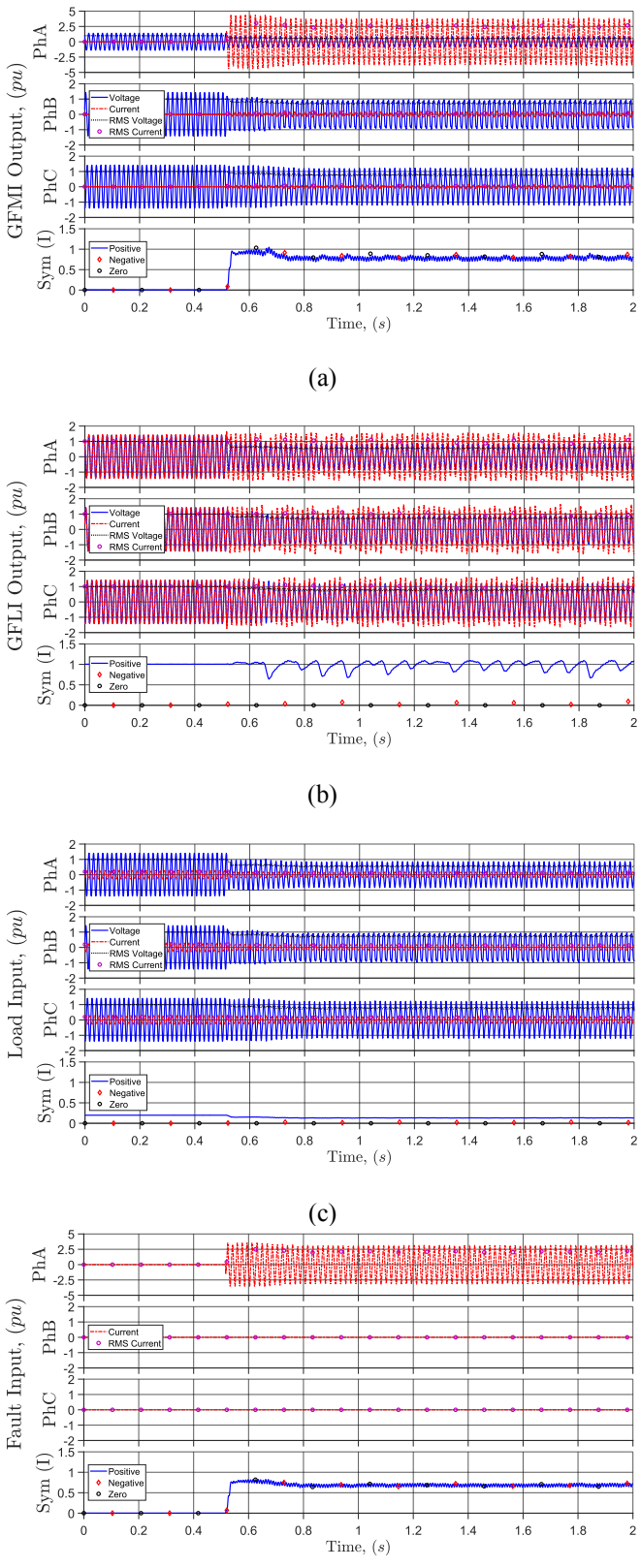

Fig. 4: Configuration A, 24 kW total load, GSF Disabled, 0.5-ohm single-line-to-ground fault on phase A applied at 0.5 seconds with the currents measured at the: GFMI (a), GFLI (b), Load (c), Fault (d)

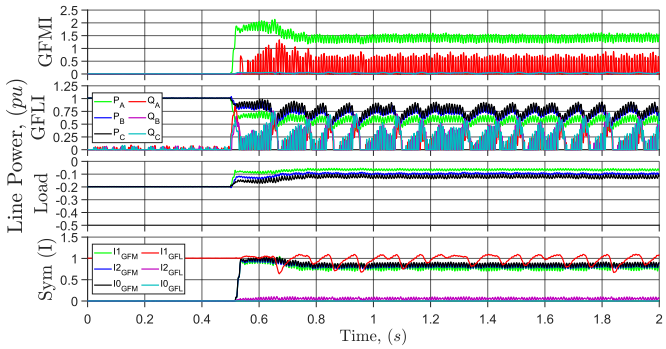

Fig. 5: Configuration A, GSF Disabled, 24kW Load, IBR and Load Power

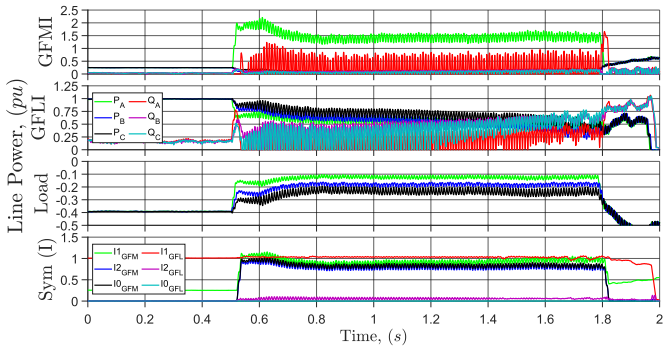

Fig. 7: Configuration A, GSF Enabled, 49kW Load, IBR, Load Power and Sequence Current Injections

0.563 p.u. on Phase A was seen and an overall fault current contribution of 2.588p.u. (with relation to the GFMI rated line current), and a GFMI contribution of 2.501 p.u. Therefore, the GFLI was able to contribute 0.36 p.u. of its rated line current to the fault with the remainder supporting the full load. While the GFLI support was minimal, the system was able to provide more current to the fault than without the GFLI, and sustain a slightly higher system voltage. Additionally, it can be seen that the GFMI provided practically all of the negative- and zero-sequence current with the GFLI only outputting a minimal amount (less than 0.05 p.u.). In a system with low short-circuit current capability, such as a purely IBR system, non-positive-sequence currents can play a vital role in protection schemes as they are a good indicator for unbalanced faults [10],[11]. Note that the current from the GFMI is measured after the delta-wye transformer, so the zero-sequence current is actually being provided by the transformer and not the GFMI. A curious note is that the GFLI's output current is modulated throughout the fault. This has been seen in previous tests [9], such as low voltage ride-through testing and phase jumps when this IBR is near the point of tripping. This is due to the fact that the phase-locked loop used to synchronize the GFLI is not able to sustain synchronization. This can be seen in Fig. 5, where the GFLI is intermittently producing reactive power while the VV function is disabled.

For the remainder of the tests, 49 kW of total resistive load was used. At this point, all GSFs were still disabled within the GFLI. Fig. 6 shows the results from this test case. Due to the increase in load, the system voltage dropped to 0.481 p.u., and had a total fault current of 2.329 p.u. of the GFMI line current rating. Additionally, the GFMI contributed 2.307 p.u. to the

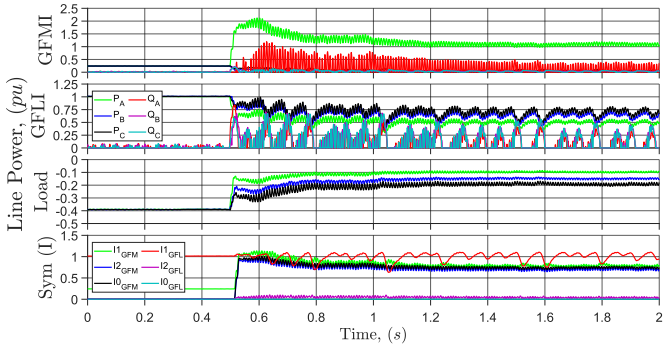

Fig. 6: Configuration A, GSF Disabled, 49kW Load, IBR, Load Power and Sequence Current Injections

fault. Therefore the GFLI contributed little to the fault, however, most of the load was supported by the GFLI, allowing the GFMI to provide more current to the fault.

Next, VV and FW were enabled on the GFLI. With the FW curve operating such that at nominal frequency the GFLI operates at rated power, the initial response of the inverter was similar to the tests with GSF disabled. However, as the fault progressed the VV function began to kick in and produce reactive power to try to boost the system voltage, reducing the real power generation of the GFLI. With a FW curve that sets the GFLI to operate at 0.5 p.u. at nominal frequency, at the initialization of the fault, the inverter quickly jumps up in real power until the VV catches up and starts driving the inverter to inject reactive power into the system. Because the two FW cases were very comparable due to the reactive power priority of the device, future tests with GSFs enabled only refer to the rated power operation case. When comparing what the voltage settled to during the fault, it was noticed that there was around a 6.5% increase in bus voltage when GSF was enabled. The total fault current was 2.545 p.u. of the GFMI line current rating, and was fully supported by the GFMI. The current magnitude of the GFMI was greater than the fault current, due to the absorption of reactive power produced by the GFLI, covering a small portion of the load. While this increase is minimal, it does show that even with a low GFLI to GFMI ratio the GSF could assist the main generation during a fault. Interestingly following the removal of the fault, the GFLI tripped due to an overvoltage event, which did not occur in the tests without GSF. The VV function of the GFLI still produced reactive power following the fault, as seen in Fig. 7, and drove the GFMI voltage up until the point that the GFLI tripped. This is a good demonstration of how too slow of a response or too aggressive of a grid support function could be detrimental in a low inertia system.

B. Configuration B

Following the single bus tests, the IBRs were separated into two buses using an inductor bank to emulate a 500 m line length between the devices. To start, the fault was implemented on the GFLI bus, with the load on the GFMI bus. Like the single bus tests, the GFLI was initially operated without GSF enabled, and set to operate at rated power. The first observation is that the GFMI supplied less current to the fault than in the Configuration A tests. The total fault current was 1.958 p.u. of the GFMI rated line current, and was fully supplied by the GFMI, with the GFMI providing very little to the load. This is seen in Fig. 8 where the GFMI Phase A real power peaked at 1.5 p.u. of the line rating,

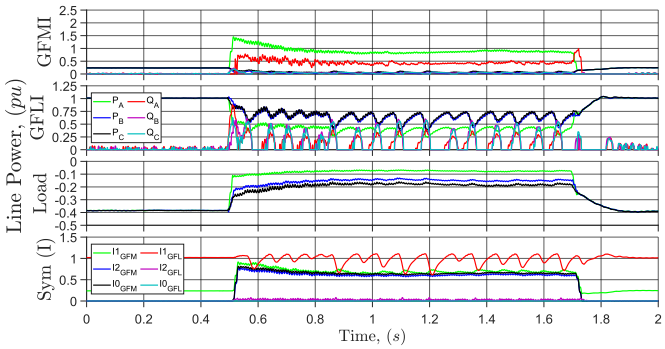

Fig. 8: Configuration B, GSF Disabled, 49kW Load, IBR, Load Power and Sequence Current Injections

compared to the 2 p.u. output of the single bus scenario. Additionally, the settled power level of the GFMI was less than the single bus cases. Looking at the results in more detail, it was found that while the GFMI bus voltage was identical to the single bus test, however the GFLI bus voltage was over 6% lower due to the additional line length. Due to the fixed resistance of the fault and the drop in bus voltage, the observed fault current is reduced when compared to tests performed in Configuration A. Beyond these observations, the dynamics of the IBRs were very consistent with those seen in the Configuration A tests and continued on this trend throughout the remainder of the testing.

The same system was then evaluated with GSF enabled. The results for this test are shown in Fig. 9. Like the Configuration A test, the same VV profile was used, however only the rated power FW profile was used. The bus voltages were once again analyzed to determine how the GSF assisted during the fault. In this test case, the bus voltages were greater than the case without GSF enabled, with the voltage increased by around 6% on both busses. With the GSF enabled, the GFLI bus voltage was now near the Configuration A disabled GSF fault voltage with the GFMI bus being sustained at a greater voltage. Additionally, the total fault current was 2.238 p.u. of the GFMI rated line current, which is lower than either of the Configuration A tests. So, while having GSFs enabled helps the system voltage, if the fault is furthest away from the primary source, little benefit is seen.

C. *Configuration C*

For the final series of tests, the locations of the load and fault were swapped. Once again the system was set with the GFLI to operate at rated power with GSFs disabled. Fig. 10 shows the results for the GFMI side fault without GSFs enabled. With the

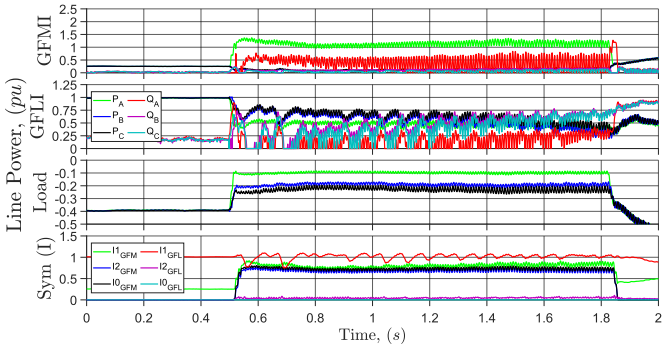

Fig. 9: Configuration B, GSF Enabled, 49kW Load, IBR, Load Power and Sequence Current Injections

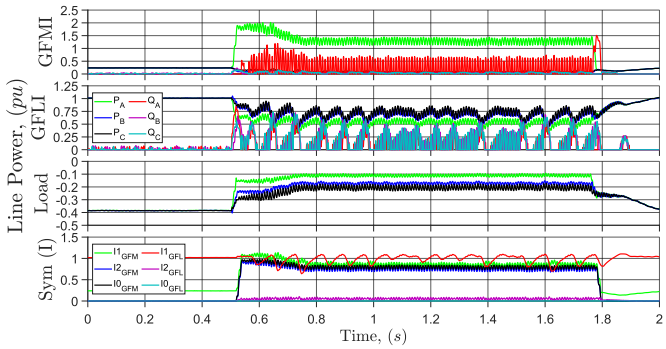

Fig. 10: Configuration C, GSF Disabled, 49kW Load, IBR, Load Power and Sequence Current Injections

fault applied, it was observed that the voltage of both buses was between 3.5-4.5% greater than the Configuration A GSF-disabled case, and both bus voltages were quite close to each other. The total fault current observed was 2.404 p.u. of the GFMI rated line current being fully supported by the GFMI. Like the Configuration B disabled GSF test, little support was given to the load from the GFMI.

After enabling the GSFs, the voltage level of the busses saw an additional 1-4.5% increase during the fault. Moreover, the voltages of both buses were very balanced with little deviation between the two. With a fault current of 2.497 p.u. of the GFMI rated line current, the system produced nearly as much fault current as the Configuration A case with less load. Interestingly, because the VV function was enabled, the GFLI could not fully support the load as it was supplying reactive power. So, although there was current being provided to the load by the GFMI and subsequently through the inductor bank, the reactive power compensation from the GFLI was able to help boost both bus voltages. The results for this final test case are shown in Fig. 11.

V. Conclusion

While we are still a long way away from a purely IBR utility, it is important to know how these devices act under abnormal conditions. By understanding how these devices interact during faults, we can figure out how to tune different technologies to assist during a fault and determine what needs to be looked for to protect the utility. Because IBRs are current-limited, traditional protection schemes cannot be used.

From this study, a few things were observed. First, if a GFLI does not have GSFs and the fault is far away from the main source, the bus voltage is significantly reduced, even when the

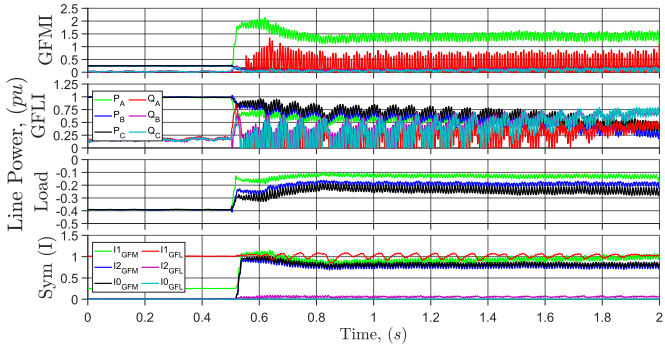

Fig. 11: Configuration C, GSF Enabled, 49kW Load, IBR, Load Power and Sequence Current Injections

GFLI is on the same bus and producing power. Following this, if GSFs can be enabled, not only can the GFLI help support the bus voltage, but also help support the system overall. Furthermore, if the fault is closer to the main source, the current sourcing nature of the GFLI can help support the load and allow for the main source to provide fault current.

While GSFs can potentially provide support during a fault on a low inertia system, it should be noted that the recovery from the fault is as important as the fault itself. When a fault is cleared or removed, it is crucial that the voltage and frequency reference return to pre-fault conditions as smoothly as possible. When GSFs are disabled, only the main source is trying to regulate the reference. However, when GFLIs are using GSFs such as FW and VV, they are also trying to regulate the reference as well. If The GFLI is set to respond very slowly, or the GSFs are too aggressive when the fault is cleared, the GFLI will continue to output reactive current that was meant to boost the voltage during the fault and subsequently continue to drive the voltage of a low inertia system until the VV profile catches back up or significant GFLIs trip and the system can reach stability. Since GFLIs may be the majority for generation on an IBR system, it is crucial that these devices do not trip following the clearing of a fault, as the system could collapse if the load is too great. Therefore having an understanding of how GSFs should be set so that GFLIs can both support the system during a fault and recover properly afterward is very important.

VI. Acknowledgment

Sandia National Laboratories is a multi-mission laboratory managed and operated by National Technology and Engineering Solutions of Sandia, LLC., a wholly owned subsidiary of Honeywell International, Inc., for the U.S. Department of Energy's National Nuclear Security Administration under contract DE-NA-0003525.

VII. References

[1] James Keller and B. Kroposki. Understanding fault characteristics of inverter-based distributed energy resources. No. NREL/TP-550-46698. National Renewable Energy Lab. (NREL), Golden, CO (United States), 2010.

[2] S. Gonzalez, N. Gurule, M. J. Reno, and J. Johnson, "Fault Current Experimental Results of Photovoltaic Inverters Operating with Grid-Support Functionality," 2018 IEEE 7th World Conference on Photovoltaic Energy Conversion (WCPEC) (A Joint Conference of 45th IEEE PVSC, 28th PVSEC & 34th EU PVSEC), 2018, pp. 1406-1411, doi: 10.1109/PVSC.2018.8547449.

[3] N. S. Gurule, J. Hernandez-Alvidrez, M. J. Reno, A. Summers, S. Gonzalez, and J. Flicker, "Grid-forming Inverter Experimental Testing of Fault Current Contributions," 2019 IEEE 46th Photovoltaic Specialists Conference (PVSC), 2019, pp. 3150-3155, doi: 10.1109/PVSC40753.2019.8980892.

[4] N. S. Gurule, J. Hernandez-Alvidrez, R. Darbali-Zamora, M. J. Reno, and J. D. Flicker, "Experimental Evaluation of Grid-Forming Inverters Under Unbalanced and Fault Conditions," IECON 2020 The 46th Annual Conference of the IEEE Industrial Electronics Society, 2020, pp. 4057-4062, doi: 10.1109/IECON43393.2020.9254562.

[5] R. Darbali-Zamora, J. Johnson, N. S. Gurule, M. J. Reno, N. Ninad, and E. Apablaza-Arancibia, "Evaluation of Photovoltaic Inverters Under Balanced and Unbalanced Voltage Phase Angle Jump Conditions," 2020 47th IEEE Photovoltaic Specialists Conference (PVSC), 2020, pp. 1562-1569, doi: 10.1109/PVSC45281.2020.9300604.

[6] N. S. Gurule, J. A. Azzolini, R. Darbali-Zamora, and M. J. Reno, "Impact of Grid Support Functionality on PV Inverter Response to Faults," 2021 IEEE 48th Photovoltaic Specialists Conference (PVSC), 2021, pp. 1440-1447, doi: 10.1109/PVSC43889.2021.9518953.

[7] Lin, Yashen, et al. Research roadmap on grid-forming inverters. No. NREL/TP-5D00-73476. National Renewable Energy Lab.(NREL), Golden, CO (United States), 2020.

[8] W. Du et al., "Modeling of Grid-Forming and Grid-Following Inverters for Dynamic Simulation of Large-Scale Distribution Systems," in IEEE Transactions on Power Delivery, vol. 36, no. 4, pp. 2035-2045, Aug. 2021, doi: 10.1109/TPWRD.2020.3018647.

[9] J. Johnson et al., "Distribution Voltage Regulation Using Extremum Seeking Control With Power Hardware-in-the-Loop," in IEEE Journal of Photovoltaics, vol. 8, no. 6, pp. 1824-1832, Nov. 2018, doi: 10.1109/JPHOTOV.2018.2869758.

[10] Buigues, G., et al. "Microgrid Protection: Technical challenges and existing techniques." International Conference on Renewable Energies and Power Quality. Vol. 1. 2013.

[11] Hassan Nikkhajoei and Robert H. Lasseter. "Microgrid fault protection based on symmetrical and differential current components." Power system engineering research center (2006): 71-74.

[12] M. J. Reno, S. Brahma, A. Bidram, and M. E. Ropp, “Influence of Inverter-Based Resources on Microgrid Protection: Part 1: Microgrids in Radial Distribution Systems,” IEEE Power and Energy Magazine, 2021.

[13] S. S. Venkata, M. J. Reno, W. Bower, S. Manson, J. Reilly and G. W. Sey Jr. “Microgrid Protection: Advancing the State of the Art,” Sandia National Laboratories, SAND2019-3167, 2019.

[14] B. Reimer, T. Khalili, A Bidram, M. J. Reno, and R. C. Matthews, “Optimal Protection Relay Placement in Microgrids,” IEEE Kansas Power and Energy Conference (KPEC), 2020.

[15] J. A. Azzolini and M. J. Reno, “Analyzing PV Hosting Capacity under Time-Varying Inverter Fault Response”, IEEE Photovoltaic Specialists Conference (PVSC), 2022.